RSC Advances

PAPER

View Article Online
View Journal | View Issue

Cite this: *RSC Adv.*, 2023, **13**, 20941

Coconut power: a sustainable approach for the removal of Cr^{6+} ions using a new coconut-based polyurethane foam/activated carbon composite in a fixed-bed column

Tomas Ralph B. Tomon,[ab] Renz John R. Estrada,[a] Rubie Mae D. Fernandez,[ab] Rey Y. Capangpangan,[c] Alona A. Lubguban,[d] Gerard G. Dumancas,[e] Arnold C. Alguno,[ag] Roberto M. Malaluan,[af] Hernando P. Bacosa[ab] and Arnold A. Lubguban *[af]

To attain efficient removal of hexavalent chromium (Cr^{6+}) from aqueous solutions, a novel polyurethane foam-activated carbon (PUAC) adsorbent composite was developed. The composite material was synthesized by the binding of coconut shell-based activated carbon (AC) onto a coconut oil-based polyurethane matrix. To thoroughly characterize the physicochemical properties of the newly developed material, various analytical techniques including FTIR spectroscopy, SEM, XRD, BET, and TGA analyses were conducted. The removal efficiency of the PUAC composite in removing Cr^{6+} ions from aqueous solutions was evaluated through column experiments with the highest adsorption capacity of 28.41 mg g^{-1} while taking into account variables such as bed height, flow rate, initial Cr^{6+} ion concentration, and pH. Experimental data were fitted using Thomas, Yoon-Nelson, and Adams-Bohart models to predict the column profiles and the results demonstrate high breakthrough and exhaustion time dependence on these variables. Among the obtained R^2 values of the models, a better fit was observed using the Thomas and Yoon-Nelson models, indicating their ability to effectively predict the adsorption of Cr^{6+} ions in a fixed bed column. Significantly, the exhausted adsorbent can be conveniently regenerated without any noteworthy loss of adsorption capability. Based on these findings, it can be concluded that this new PUAC composite material holds significant promise as a potent sorbent for wastewater treatment backed by its excellent performance, cost-effectiveness, biodegradability, and outstanding reusability.

Received 5th April 2023
Accepted 5th July 2023

DOI: 10.1039/d3ra02266h

rsc.li/rsc-advances

1. Introduction

The Earth has continuously faced significantly challenging threats, including global warming, air pollution, rising human population, and water contamination.[1] Today, the accessibility to clean drinking water has become scarce in most parts of the world. This has drastically affected human civilization's environmental, social, and economic conditions.[2] Data presented by the World Health Organization (WHO) and the United Nations Children's Fund (UNICEF) in 2017 estimated that only 71% of the world population has access to safe drinking water. A study conducted by the Global Burden of Diseases (GBD) in the same year shows that unsafe water source ranks 15th in the causes and risk factors for death and diseases, responsible for about 1.23 million annual deaths worldwide, and approximately 5507 annual deaths in the Philippines. Excessive release of pollutants such as toxic metal ions,[3] dye effluents,[1] and excessive use of pesticides and inorganic fertilizers[4] into waterways from various industries contributes significantly to pollution and poses an imminent threat to living organisms.[1]

Heavy metals are metals with high densities and are toxic even at low concentrations. These pollutants enter various ecosystems through different natural and anthropogenic activities.[5] Global industrialization[6] and the rapid increase in the world population enabled hazardous materials to spread into the environment at unprecedented speed. Building materials, mining operations, leather tanning, and electronics are some of

[a]*Center for Sustainable Polymers, Mindanao State University – Iligan Institute of Technology, 9200 Iligan City, Philippines. E-mail: arnold.lubguban@g.msuiit.edu.ph*
[b]*Graduate Program of Environmental Science, Department of Biological Sciences, Mindanao State University – Iligan Institute of Technology, 9200 Iligan City, Philippines*
[c]*Department of Physical Sciences and Mathematics, Mindanao State University at Naawan, 9023 Naawan, Philippines*
[d]*Department of Mathematics, Statistics, and Computer Studies, University of the Philippines, Rural High School, Paciano Rizal Bay, 4033 Laguna, Philippines*
[e]*Department of Chemistry, The University of Scranton, Scranton, PA 18510, USA*
[f]*Department of Chemical Engineering and Technology, Mindanao State University – Iligan Institute of Technology, 9200 Iligan City, Philippines*
[g]*Department of Physics, Mindanao State University – Iligan Institute of Technology, 9200 Iligan City, Philippines*

the few industries utilizing heavy metals.[7,8] Due to a serious lack of compliance with the regulations with regards to discharges[8] of industrial processes, heavy metals spread into the environment[9] through untreated wastewater[10] in the form of solids, liquids, and gases. It is estimated that two million tons of sewage and other effluents are being drained into the bodies of water daily.[2,11] Heavy metals are known to be human carcinogens and are non-biodegradable.[6,12] As such, heavy metals tend to bioaccumulate and produce genotoxic, carcinogenic, and mutagenic effects in plants and animals, which in turn, can be assimilated by the human body through ingestion, making them a more significant threat as their exposure continues to grow, especially in less developed countries.[2]

Chromium is one of the most common heavy metals that pollute the environment, apart from arsenic, cadmium, copper, nickel, lead, and mercury. It is known for its anti-corrosive properties and is the primary additive in stainless steel manufacturing industries. It is used primarily in wood preservation, leather tanning, metal finishing, and pigmentation. Chromium exists and enters different environmental media *via* two oxidation states: trivalent (Cr^{3+}) and hexavalent (Cr^{6+}) chromium, stable[13–15] yet considered toxic and carcinogenic pollutants. The trivalent state of chromium that occurs in nature is essential for glucose metabolism in mammals.[16] The hexavalent state is considered the most toxic state among the chromium species because of its transportability and absorbability within the cell. Cr^{6+} is reduced through metabolic processes where genotoxic damage and other forms of toxicity are generated.[17] Because of this, international and national legislative bodies standardized the permissible tolerance limits for different types of heavy metals that are environmentally safe. This mandates the effective treatment of heavy metals and other pollutants before they can be discharged into the environment.

Various conventional treatment methods, such as chemical precipitation, ion exchange, evaporation, and biological treatment were reported to remove Cr^{6+} ions from water effectively.[5,18,19] However, these methods have several drawbacks including high energy consumption, high operational cost and maintenance, high chemical input, and the possibility of generating secondary pollutants. Adsorption, on the other hand, has been considered one of the promising wastewater treatment methods[20,21] because of its simple application, low operational cost, reusability, low energy consumption, and good removal performance. Because of this, the focus was shifted towards an adsorption-based approach, wherein characteristics mainly depend on high porosity and surface-charge distribution of the adsorbent.[1] As a result, recent studies related to the development of technologies that are sustainable and efficient in adsorbing heavy metals from aqueous solutions continue to take place.

Commercial activated carbon (AC) is the most commonly utilized adsorbent for wastewater treatment. However, it has limiting factors as it is inherently costly, non-renewable, challenging to recover, and tends to break down into pieces and finer fragments, making its practical deployment difficult. Additionally, synthetic polymers are also commonly employed in wastewater treatment processes[22] in the form of polyurethane (PU) foams. Due to their excellent porosity distribution and high surface area, PU foams are known for their many applications in various fields, such as appliances, industrial, medical, and filtration systems. Despite this, the polyols used for the production of PU foams are derived from non-renewable resources and are expected to last for only a few more years.[23] Thus, choosing the right raw material is critical, and favoring bio-based materials as an alternative source for producing PU foams is essential.[24]

Biopolyols are the potential alternative raw materials for the sustainable production of rigid PU foam, but in order to do so, polyols would require a relatively high hydroxyl value.[17] Vegetable oils do not naturally contain hydroxyl groups and are less suitable reactants in polyols production than other substrates unless chemical modifications are made.[18] Hydroxyl groups are therefore chemically generated from vegetable oils, the number of which is dependent on the nature and triglyceride structure of the specific oil. Unsaturated vegetable oils are typically modified by double bond epoxidation and ring-opening reactions with alcohols and haloacids.[5,6,19] Saturated vegetable oils usually undergo transesterification and amidation reactions.[11,20–23] However, previous studies on saturated vegetable oil modification reported polyols with low hydroxyl values, which necessitates petroleum-based polyol replacement to be effective for use in rigid PU foam formation.[24,25] This major limitation is attributed to the mostly unsaturated composition of vegetable oil triglycerides making it less capable of hydroxyl functionalization.[6]

Coconut is one of the most abundant and inexpensive commodities available in the Philippines and its neighboring countries. Alongside the production of goods from coconut for exportation is the increased production of wastes and their by-products. To solve this difficulty, the present study was geared to address this problem and investigate the utilization of coconut-based polyurethane foam-activated carbon (PUAC) composites for the effective removal of Cr^{6+} contaminants in wastewater bodies. These coconut-oil-based PUAC are designed to be thermally and chemically stable,[25] and inexpensive to generate due to their raw materials being considered as waste or low-value by-products. Additionally, the functional groups present in the composite material was analysed using fourier transform infrared spectrometer (FTIR). The enhancement of the surface area of the composite was characterized using scanning electron microscopy (SEM), and surface area analyzer. The thermal stability and microstructural properties were determined using a thermal gravimetric analysis (TGA), and X-ray diffraction (XRD) analyses, respectively.

Moreover, the effects of several operational parameters, including bed height, flow rate, influent Cr^{6+} concentration, pH, and reusability studies were examined and the experimental data were fitted using various models to predict the breakthrough curves for the dynamic adsorption of Cr^{6+} onto the PUAC foam composites.

2 Experimental

2.1 Materials

The AC sourced from coconut shells was supplied by the Philippine Japan Active Carbon. AC was pulverized and sieved using

a 50-mesh screen to attain a uniform size. The potassium dichromate ($K_2Cr_2O_7$) used in this study was of analytical grade and was provided by Caraga State University (CSU, Butuan City, Philippines). Materials such as the catalyst (Polycat® 8) and surfactant (INV® 690) were obtained from Sigma-Aldrich Chemicals, Philippines. The polyol component used was a coconut oil-based polyol (in-house, patent-pending) blended with a fraction of petroleum-based polyol (Voranol® 4701, polyether polyol). Voranol® 4701, a stabilizer, dispersant silicon oil, and methylene diphenyl diisocyanate (MDI, PAPI 135 SH), were provided by Chemrez Technologies, Inc. (Quezon City, Philippines). The abaca fiber used as a cellular reinforcement was locally sourced in Iligan City, Philippines.

2.2 Synthesis of the coconut oil-based polyol

The coconut oil-based polyol used in this study was previously developed[26] through a sequential process of (1) breaking down coconut triglycerides into its component acylglycerol by-products (180 °C, 3 h) under constant stirring, followed by a (2) polyol-forming process (200 °C, 3 h). The polyol product was then allowed to cool down at room temperature and stored in a sealed glass container.

2.3 Preparation of adsorbate solution

A stock solution of 1000 ppm of Cr^{6+} was prepared by dissolving 2.8286 g of $K_2Cr_2O_7$ in 1000 mL distilled water and stored in amber glass. This study obtained the required concentrations by successive dilution of the standard stock solution (0–300 ppm). Adsorption experiments at different concentrations of Cr^{6+} were performed using the prepared solutions.

2.4 Preparation of the composite PU foam

To synthesize the foam, A-side (MDI) and B-side (polyol and formulation components) materials were mixed using the free-rise method.[27] To impregnate the PU foam with AC, a reaction occurred between the components, wherein one NCO end of the MDI reacted with the surface –OH group of the AC, while the other end reacted with the OH functional groups in the polyol chain.[28]

The polyol mixture (B-side components) containing the polyols, surfactant, and catalyst was mixed with a substantial amount of activated carbon at 1000 rpm for 60 seconds to produce the polyol mixture. A stoichiometric amount of MDI (A-side component) was then added to the reaction mixture with the same rotation speed for another 15 seconds to obtain a homogeneous mixture. Once homogenized, the mixture was left undisturbed and was allowed to rise freely. The resulting expanded polymer was then continuously cured in an oven at 60 °C for two (2) hours.[29] After the curing process, the foam samples were set aside overnight before cutting into a 0.5 × 0.5 × 0.5 cm cube dimensions and were consequently tested.

2.5 Column adsorption studies

Fig. 1 depicts the actual layout of the fixed-bed column setup. The adsorption experiment of the adsorbate solution was carried out in a continuous experimental system on a laboratory scale made of an acrylic column with an inner dimension of 2 cm in diameter and 20 cm in height. The entire process was completed at room temperature. One (1) g cm^{-1} of the PUAC composite was weighed and packed into the column. The column was supported with a 3D-printed funnel on both ends to ensure stability and proper distribution of the inlet solution, as seen in the figure.

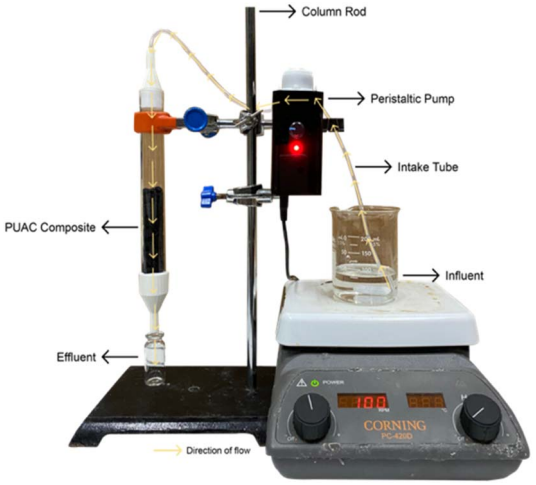

Fig. 1 Actual setup of the fixed-bed column.

The adsorbent was then added from the top of the column and carefully packed until the desired height was attained. The solution containing the desired concentration of Cr^{6+} ions was stirred constantly at 100 rpm and pumped through the continuous system in a down-flow mode with the aid of a peristaltic pump. Aliquots were collected at different time intervals, and the concentration of the output solution was measured spectrophotometrically using a UV-Vis spectrometer at 313 nm wavelength (Thermo Fisher Scientific Genesys 10s, MA USA).[30]

Experiments were performed to examine the impact of flow rate and bed height on the adsorption of Cr^{6+} ions onto the PUAC. The tests were conducted at three (3) flow rates (4, 6, and 8 mL min^{-1}), three (3) bed heights (5, 10, and 15 cm), and three (3) pH values (2, 4, and 6), respectively while keeping other variables constant. Following the optimization of flow rate, bed height, and pH, the study assessed the impact of metal ion concentration on adsorption efficiency at concentrations of 50, 100, and 200 mg L^{-1}.

The fixed-bed setup experiment was carried out until the saturation point at which no adsorption of Cr^{6+} ions is detected. The breakthrough curves were established as it is a vital characteristic in determining a fixed-bed column's dynamic response.[3] Breakthrough curves are expressed by C_t/C_0 against time t.

2.6 Column data analysis

The breakthrough curve represents the performance of the fixed-bed column. The total mass adsorbed, q_{total}, at certain conditions against time t and was calculated using eqn (1).

$$q_{\text{total}} = \frac{QA}{1000} = \frac{Q}{1000}\int_0^{t_{\text{total}}} C_{\text{ad}}\,\mathrm{d}t \quad (1)$$

where Q is the influent flow rate (mL min^{-1}), A is the area under the curve, t is the total run time (min), and C_{ad} is the adsorbed Cr^{6+} ions concentration in mg L^{-1}.

The maximum metal uptake, q_{eq}, of the adsorbent using the continuous system was calculated using eqn (2). Finally, the total volume of the effluent, V_{eff}, was calculated using eqn (3).

$$q_{\text{eq}} = \frac{q_{\text{total}}}{m} \quad (2)$$

$$V_{\text{eff}} = Qt_{\text{total}} \quad (3)$$

where m is the dry weight of the adsorbent in the continuous system.

2.7 Column breakthrough curve modeling

Several theoretical adsorption models have been applied to project the dynamic adsorption behavior of the residual Cr^{6+} ions in a fixed-bed column. In this work, three of the most commonly applied mathematical models, namely the Adams-Bohart model, Thomas model, and Yoon-Nelson model, were used to establish fit with the experimental data.

The Adams-Bohart[31] model is grounded on the surface reaction theory and describes the relationship between C_0/C_t against time t in a continuous system and assumes that equilibrium is not attained instantaneously.[3] The linear form of the Adams-Bohart model can be demonstrated as:

$$\ln\left(\frac{C_t}{C_0}\right) = k_{\text{AB}}C_0t - k_{\text{AB}}N_0\left(\frac{Z}{U_0}\right) \quad (4)$$

where k_{AB} = Adams-Bohart rate constant (L mg^{-1} min^{-1}); N_0 = saturation concentration (mg L^{-1}); t = flow time (min); Z = bed height (cm); and U_0 = superficial velocity (cm min^{-1}). The plot of $\ln(C_t/C_0)$ against time t was used to determine the values of k_{AB} and N_0.

In designing a continuous adsorption column, determining the maximum adsorption capacity, q_{Th}, is essential. The Thomas[32] model is one of the most common tools. This model assumes that mass transfer at the interface controls adsorption rather than chemical interactions between molecules.[33] The linear form of the equation is expressed as:

$$\ln\left(\frac{C_0}{C_t} - 1\right) = \frac{k_{\text{Th}}q_{\text{Th}}m}{Q} - k_{\text{Th}}C_0t \quad (5)$$

where k_{Th} = is the Thomas rate constant (L mg^{-1} min^{-1}); q_{Th} = adsorption capacity (mg g^{-1}); t = total flow time (min); m = mass of the adsorbent (g); and Q = flow rate (mL min^{-1}). By plotting the $\ln[(C_0/C_t) - 1]$ against time t, the values for k_{Th} and q_{Th} can be calculated based on the slope and intercept, respectively.

The Yoon-Nelson[34] model is also a common tool in determining the breakthrough and saturation time of the continuous system. The model assumes that the adsorption rate of each adsorbate is proportional to the rate of decrease in adsorption.[35] The model is given as

$$\ln\left(\frac{C_t}{C_0 - C_t}\right) = k_{\text{YN}}t - \tau k_{\text{YN}} \quad (6)$$

where k_{YN} = Yoon–Nelson rate constant (min^{-1}); τ = time required for 50% adsorbate breakthrough (min); and t is the breakthrough time. The value of k_{YN} and τ is evaluated from the slope and intercept of the linear plot of $\ln[C_t/(C_0 - C_t)]$ against t.

2.8 Characterization

To study the functional groups and the surface morphology of the synthesized PUAC, the samples were characterized using FTIR (Shimadzu ATR-FTIR IRTracer-100, Kyoto, JPN), SEM (JEOL JSM-6510LA, Tokyo, JPN). The specific surface area and pore diameter of the adsorbent were measured by utilizing a surface area analyzer (Microtrac BELSORP MINI X, Osaka, JPN). The thermal degradation profile was analyzed using TGA (Shimadzu DTG 60H, Kyoto, JPN) with nitrogen ambient (flow rate 20 mL min^{-1}) and a temperature rate of 10 °C min^{-1}. All pH values were measured using a digital pH meter (KEM AT-710, Kyoto, JPN). The XRD patterns were recorded with a Cu Kα radiation source (40 kV and 30 mA) in a 3–60° 2θ range with a speed of 0.02° 2θ/0.60s (Shimadzu XRD Maxima 7000, JPN). The open-cell content of the foam was obtained using a pycnometer (Quantachrome ULTRAPYC 1200e, FL USA) and calculated as:

$$\text{Open\%} = \frac{v_{\text{g}} - v_{\text{p}}}{v_{\text{g}}} \times 100 \quad (7)$$

where v_{g} = is the geometric volume and v_{p} = is the pycnometric volume.

3 Results and discussion

3.1 Characterization of the adsorbent

3.1.1 FTIR analysis. To ascertain the chemical interaction that is present between the AC and PU matrix, the FTIR spectra in the 400 to 4000 nm wavelength range, was utilized. As shown in Fig. 2, the strong IR bands in the blank PU foam are between 1070 cm^{-1} and 1132 cm^{-1}, 3357 cm^{-1}, and 1730 cm^{-1}, which are assigned to the C–O, NH, and C=O bonds present in the region, respectively. At ~1599 cm^{-1}, the peak intensity specific to C=C was reduced in PUAC. This indicates that the NCO functionality of MDI had reacted with the surface hydroxyls of AC through –NCO and –OH reaction, forming the carbamate bond.[26,36] Further, the peak between 1070 cm^{-1} and 1132 cm^{-1} and that of the N–H peak at 3357 cm^{-1} became noticeably weak compared to the blank PU. The observed weak peak intensities imply that hydrogen bonding occurred, confirming the incorporation of AC into the composite material. This is attributed to the heterogeneity of the carbonyl environments, which substantiates the linkage between the AC and the polymer.[28] Finally, the evident presence of the carboxylic (1730 cm^{-1}) and hydroxylic (3357 cm^{-1}) functional groups acted as proton donors, and are ultimately responsible for the uptake of heavy metals.[35,36]

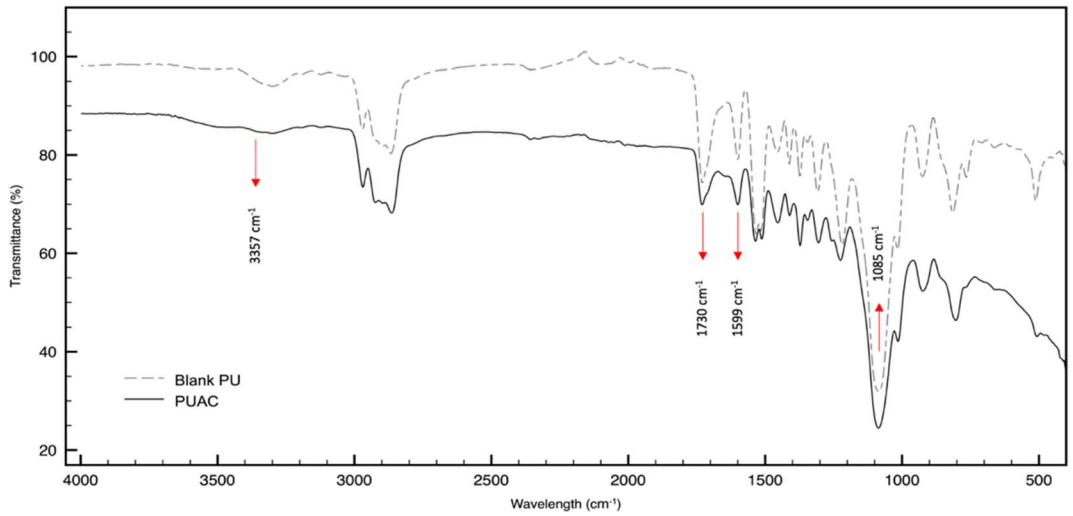

Fig. 2 FTIR spectra of a blank polyurethane foam against the composite foam.

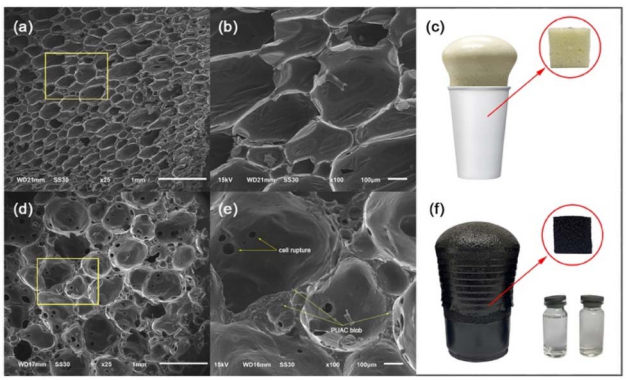

Fig. 3 SEM image of (a) blank polyurethane (PU, 1 mm), (b) blank PU (100 μm), (c) blank PU cup foam, (d) polyurethane foam-activated carbon (PUAC, 1 mm), (e) PUAC (100 μm), (f) PUAC cup foam and resulting clear effluent after column adsorption.

3.1.2 SEM and pycnometric analysis. As illustrated in Fig. 3(b), SEM surface morphology analysis revealed that the addition of AC exhibited a nearly homogeneous, and well-developed open-cell structure. The open-cell content was increased by approximately 13% compared to PU with a recorded average rate of 88%. The findings are consistent with similar research,[28,37,38] which also suggests that increase in open-cell content can lead to an increase in adsorption capacity by providing a more extensive surface area for adsorption. Furthermore, the analysis has also revealed a significant increase in the surface roughness of PUAC with the addition of AC particles.[1,28,39,40] This implies a strong interaction between PU and AC, which corroborates the potential of the material for effective heavy metal ion adsorption.

3.1.3 Surface area analysis. A surface area analyzer was used to determine the textural parameters (specific surface area and pore size) of both blank PU and PUAC through their nitrogen BET adsorption–desorption isotherms. The results showed that the surface area of PU (1.1817 $m^2\ g^{-1}$) was lower than that of PUAC (10.8950 $m^2\ g^{-1}$). This implies that the incorporation of AC into the PU, drastically enhanced the composite's surface area, thus increasing the available sorption sites for the sequestration of Cr^{6+} ions. Additionally, the average pore sizes of PU and PUAC were found to be measuring 2.3407 nm and 0.9826 nm, respectively. Smaller pore sizes in a material lead to an increased surface area and surface-to-volume ratio,[41] explaining the observed increase in the surface area of PUAC.

3.1.4 XRD analysis. Fig. 4 depicts the XRD diffractogram of PU and the PUAC. It was revealed that the diffractograms exhibited a broad and weak diffraction peak at 19° and around 43° 2θ, corresponding to the respective diffraction of the amorphous carbon skeleton at (002) and (100) planes, respectively.[42] Further, the low-intensity occurrence of these peaks suggests a low degree of graphitization,[43] and possesses a crystalline carbonaceous structure.[42,44]

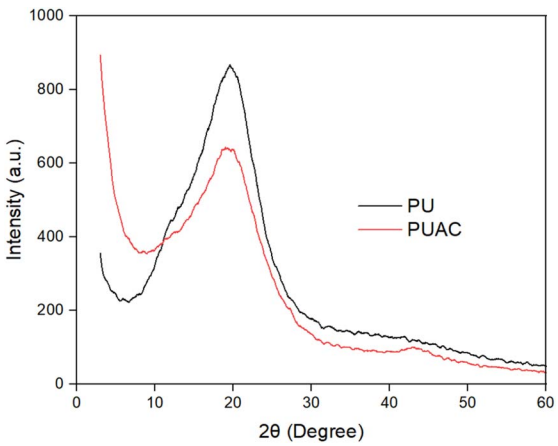

Fig. 4 XRD profile of a blank polyurethane (PU) and polyurethane foam-activated carbon composite.

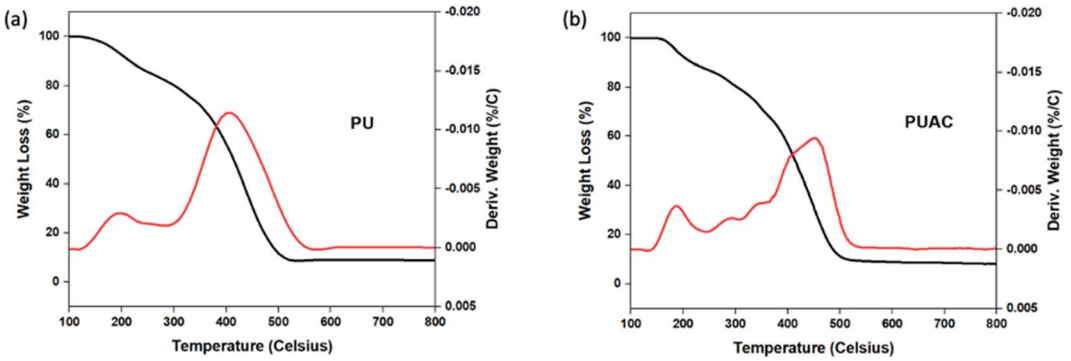

Fig. 5 TGA–DTG curves of (a) polyurethane (PU) and (b) polyurethane foam-activated carbon.

3.1.5 Thermogravimetric analysis. The thermal behavior of pristine PU and PUAC is presented in Fig. 5. As seen in the DTG curve of PU found in Fig. 5(a) reveals two endothermic peaks around 183 °C and 400 °C. These peaks correspond to the thermal decomposition of the hard and soft segments, respectively. These hard segments are attributed to the urethane bonds, while the soft segments are influenced by the fatty acid chains present in the PU matrix.[45] On another note, the DTG for the PUAC reveals multiple peaks at 184 °C, 286 °C, 341 °C, and 452 °C as shown in Fig. 5(b). Similarly with the pristine PU, the peaks at 184 °C and 452 °C represent the thermal decomposition of urethane segments and fatty acid components in the PUAC composite. Moreover, the second peak is attributed to the pyrolysis of the AC components.[43] Around the temperature range of 300 °C to 370 °C, the observed weight loss might be due to the cleavage of the hard urethane linkages leading to the formation of primary amine, terminal alkene, and CO_2.[42] Based on these findings, the PUAC formulation presented in this study does not have a significant effect on the thermal stability of the material.

3.2 Fixed-bed column studies

3.2.1 Effect of bed height in Cr^{6+} sequestration. To ascertain the effect of bed height in Cr^{6+} ion sequestration, three different bed heights were tested and measured: 5, 10, and 15 cm. The experiments were conducted under constant conditions of Cr^{6+} ion concentration at 100 mg L^{-1}, pH level of 6, and a flow rate of 4 mL min^{-1}.

Results revealed that as the bed height was increased from 5 cm to 15 cm, exhaustion time also increased from 180 to 300 min, as seen in the breakthrough curve in Fig. 6(a). These findings confirm the proportional relationship between the breakthrough curve and bed height, thus increasing mass transfer zones.[8,46] Notably, reduced bed height led to faster saturation, while increased bed height yielded higher removal efficiency of Cr^{6+} ions. An increase in bed height created more available active sorption sites and contact time, improving the interaction between the PUAC and Cr^{6+} ions, as is observed in similar studies.[35]

3.2.2 Effect of flow rate in Cr^{6+} sequestration. To evaluate the influence of flow rate on column performance, the influent containing Cr^{6+} ions was tested at different flow rates (4, 6, and 8 mL min^{-1}) while maintaining a constant bed height (10 cm), pH level (6), and initial concentration (100 mg L^{-1}).

The impact of different flow rates in the breakthrough curves were indicated in Fig. 6(b). Results showed that when the flow rate is increased, breakthrough occurs much more rapidly, leading to a decreased breakthrough time. This is because the increased flow rate promotes Cr^{6+} ions to have lesser contact time with the PUAC, ultimately reducing the removal capacity of Cr^{6+} ions in the column.

3.2.3 Effect of initial concentration in Cr^{6+} sequestration. The effect of the initial Cr^{6+} ion concentration on the adsorption

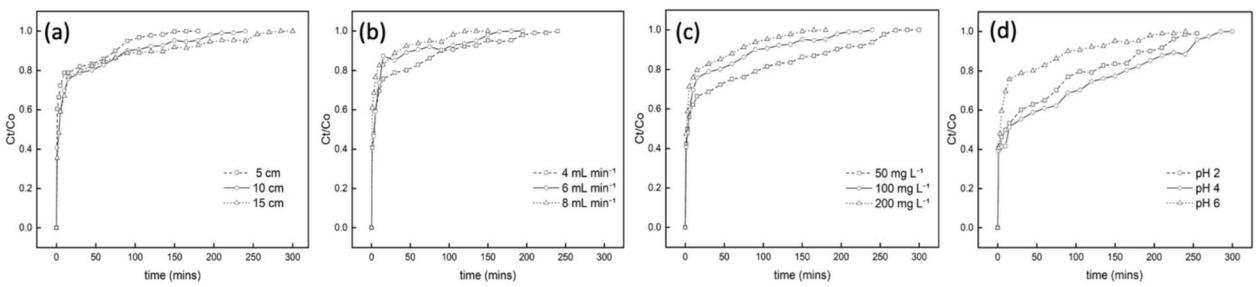

Fig. 6 (a) Effect of bed height (flow rate 4 mL min^{-1}, initial Cr^{6+} ions concentration 100 mg L^{-1}), (b) effect of flow rate (bed height 10 cm, initial Cr^{6+} ions concentration 100 mg L^{-1}) (c) effect of initial Cr^{6+} ions concentration (bed height 10 cm, flow rate 4 mL min^{-1}), and (d) effect of pH level (bed height 10 cm, flow rate 4 mL min^{-1}, initial Cr^{6+} ions concentration 100 mg L^{-1}) on the breakthrough curves for the removal of Cr^{6+} ions from aqueous media.

performance of the column was studied by varying the initial concentration from 50 mg L^{-1} to 200 mg L^{-1}. In this experiment, the adsorbent bed height (10 cm), pH level (6), and flow rate (4 mL min^{-1}) were kept constant.

Fig. 6(c) displays the inverse relationship between the initial concentration and breakthrough curve. As the initial Cr^{6+} ion concentration increases, saturation takes place faster, and the breakthrough time decreases. This is because the surface area readily available for adsorption is higher at lower initial concentrations and *vice versa*, resulting in lesser efficiency. This phenomenon occurs because an increase in the initial concentration acts as a driving force to overcome all the resistance to adsorption, resulting in an abrupt breakthrough.[47]

3.2.4 Effect of pH level in Cr^{6+} sequestration. To investigate the effect of pH levels on the Cr^{6+} uptake performance of the PUAC, different pH levels of 2 to 6 were applied while maintaining the bed height (10 cm), flow rate (4 mL min^{-1}), and initial concentration (100 mg L^{-1}) constant.

The effect of various pH levels in Cr^{6+} sequestration is shown in Fig. 6(d). It was revealed that the optimum breakthrough time (300 min) of the PUAC was observed at pH = 4. This observation might be attributed to the higher ratio of $HCrO_4^-$ and $Cr_2O_7^{2-}$ present in the adsorbate at pH = 4,[21] which could significantly induce the uptake capacity of the PUAC. In contrast, the excessive protonation of the adsorbent surface at pH = 2 disrupted the interaction between Cr^{6+} and the adsorbent,[1,44] leading to a decreased breakthrough time. Moreover, when pH was further increased from 4 to 6, there is an increased formation of CrO_4^{2-} and $Cr_2O_7^{2-}$ precipitates[3,21] which cannot be adsorbed by the PUAC, resulting in a decrease in the breakthrough time from 300 to 240 min.

3.3 Breakthrough curve modeling

Breakthrough curves obtained under various conditions can be utilized to estimate the effectiveness of a column design. To adapt lab-scale column studies for industrial use, various mathematical models have been suggested. In this research, the Adams-Bohart, Thomas, and Yoon-Nelson models were employed to select the best-fit model for predicting the columns' dynamic behavior.

3.3.1 Adams-Bohart model. The $\ln(C_t/C_0)$ values were graphed against time t to calculate the slope and intercept, which yielded k_{AB} and N_0. The obtained k_{AB} and N_0 values for all the breakthrough curves are listed in Table 1, accompanied by the corresponding correlation coefficients R^2.

The study found that the Adams-Bohart model can be used to predict the initial process of a continuous system, with high correlation coefficients obtained for the bed height and initial metal concentration breakthrough curves. However, the model's applicability decreased at higher parameters, indicating the need for an alternative approach to predict system

Table 1 Parameters of the Adams-Bohart model at varying conditions

Parameter		k_{AB} (L mg^{-1} min^{-1})	N_0 (mg L^{-1})	R^2
Bed height (cm)	5	2.2×10^{-5}	0.9151	0.816
	10	2.4×10^{-5}	0.6024	0.678
	15	1.8×10^{-5}	0.5036	0.613
Flow rate (mL min^{-1})	4	2.4×10^{-5}	0.6024	0.678
	6	2.9×10^{-5}	0.7180	0.562
	8	2.3×10^{-5}	0.7504	0.703
Initial metal concentration (mg L^{-1})	50	4.0×10^{-5}	0.4038	0.838
	100	2.4×10^{-5}	0.6024	0.678
	200	1.3×10^{-5}	0.8981	0.696
pH	2	3.1×10^{-5}	0.7042	0.678
	4	2.9×10^{-5}	0.8279	0.895
	6	2.4×10^{-5}	0.6024	0.678

Table 2 Parameters of the Thomas model at varying conditions

Parameter		k_{Th} (L mg^{-1} min^{-1})	q_{Th} (mg g^{-1})	R^2
Bed height (cm)	5	3.5×10^{-4}	0.7107	0.935
	10	2.1×10^{-4}	0.3775	0.880
	15	1.7×10^{-4}	0.3691	0.828
Flow rate (mL min^{-1})	4	2.1×10^{-4}	0.3775	0.880
	6	3.1×10^{-4}	0.3867	0.876
	8	4.3×10^{-4}	0.9726	0.912
Initial metal concentration (mg L^{-1})	50	3.5×10^{-4}	0.2707	0.930
	100	2.1×10^{-4}	0.3775	0.880
	200	1.6×10^{-4}	0.7357	0.866
pH	2	1.5×10^{-4}	0.8268	0.880
	4	1.8×10^{-4}	1.8026	0.978
	6	2.1×10^{-4}	0.3775	0.880

Table 3 Parameters of the Yoon-Nelson model at varying conditions

Parameter		k_{YN} (min^{-1})	τ_{calc} (min)	R^2
Bed height (cm)	5	3.5×10^{-2}	8.8843	0.935
	10	2.1×10^{-2}	9.4383	0.880
	15	1.7×10^{-2}	13.842	0.828
Flow rate (mL min^{-1})	4	2.1×10^{-2}	9.4383	0.880
	6	3.1×10^{-2}	6.4446	0.876
	8	4.3×10^{-2}	5.8983	0.912
Initial metal concentration (mg L^{-1})	50	1.7×10^{-2}	13.524	0.930
	100	2.1×10^{-2}	9.4383	0.880
	200	3.2×10^{-2}	9.1966	0.866
pH	2	1.5×10^{-2}	20.6707	0.880
	4	1.7×10^{-2}	45.0640	0.978
	6	2.1×10^{-2}	9.4383	0.880

behavior. Additionally, the observed decreasing trend in the rate constant, k_{AB}, for all parameters suggests that external mass transfer dominates the system kinetics, which is influenced by flow conditions and contact surface area.[48]

3.3.2 Thomas model. The results of this study demonstrate the applicability of the Thomas model, which is a commonly used approach for predicting breakthrough curves. The obtained values of k_{Th}, and q_{Th}, based on the slope and intercept along with their corresponding correlation coefficients, are presented in Table 2. According to the data presented, k_{Th} and q_{Th} decrease as the bed height and initial metal concentration increase, as observed in various studies.[7,8,35] Additionally, with the increase in flow rate, values of q_{Th} increased while decreasing in k_{Th} values. Finally, the obtained correlation coefficients for all of the analysed breakthrough curves are higher than those obtained using the Adams-Bohart model, indicating a good fit of the experimental data. This observation suggests that neither external nor internal diffusion were the rate-limiting steps.

3.3.3 Yoon-Nelson model. The values of this model were obtained from the plot of eqn (6) and were fitted to the model. The values of k_{YN} and τ were summarized in Table 3. An increase in bed height leads to a longer time for 50% adsorbate breakthrough due to slower saturation, while an increase in concentration and flow rate results in a significant decrease in τ as the column attains saturation quickly. This finding is consistent with previous research.[3,6] R^2 values suggest both Thomas and Yoon-Nelson models predict Cr^{6+} removal by PUAC in a fixed bed column.

Table 4 presents the summary of the PUAC's performance for the sequestration of Cr^{6+} ions at various adsorption parameters. It can be observed that, the more favorable adsorption performance can be observed at higher bed heights, lower flow rates, and higher initial concentrations. Moreover, the adsorption performance of other adsorbents in similar conditions are summarized in Table 5. It has been found out that the PUAC's adsorption capacity is comparable to, or even performs better compared to other adsorbents found in the literature.

Table 5 Adsorption performance of previously reported adsorbents for the sequestration of Cr^{6+} ions

Adsorbent	q_{eq} (mg g^{-1})	Reference
PUAC	28.41	This study
Activated carbon	15.5	49
Quaternized rice hulls	32.3	50
Sugarcane bagasse	2.48	51

Table 4 Parameter of the fixed bed column for the removal of Cr^{6+} ions by polyurethane foam-activated carbon (PUAC)

Initial concentration (mg L^{-1})	Bed height (cm)	Flow rate (mL min^{-1})	pH	Total time (min)	Total mass adsorbed (mg)	Equilibrium uptake (mg g^{-1})	Effluent volume (mL)
100	5	4	6	180	72	7.18	720
100	10	4	6	240	96	10.66	960
100	15	4	6	300	120	8.38	1200
100	10	4	6	240	96	10.66	960
100	10	6	6	195	117	10.56	1170
100	10	8	6	150	120	8.66	1200
50	10	4	6	300	60	9.48	1200
100	10	4	6	240	96	10.66	960
200	10	4	6	180	144	13.54	720
100	10	4	2	255	102	22.03	1020
100	10	4	4	300	120	28.41	1200
100	10	4	6	240	96	10.66	960

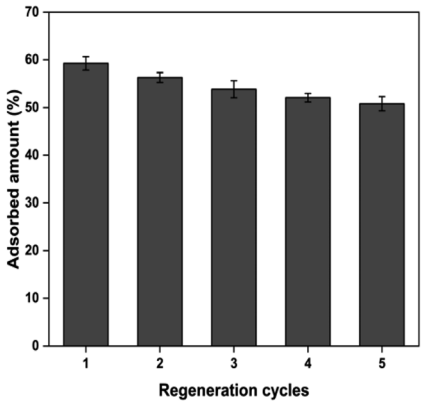

Fig. 7 The reusability of polyurethane foam-activated carbon (PUAC) for the sequestration of Cr^{6+} ions.

3.4 Regeneration studies

The adsorbent reusability is a crucial aspect in the lens of economic viability, especially in an industrial-scale setting. In the present study, the chromate-exhausted PUAC was subjected to desorption studies using a 0.1 M NaOH desorbing agent. The regeneration studies were performed by eluting the desorbing agent into the column at a flow rate of 2.5 mL min^{-1} for 30 min. The column was then rinsed with deionized water for another 30 min before employing another cycle for Cr^{6+} adsorption. After undergoing four (4) adsorption–desorption cycles, the removal efficiency of PUAC remained above 80% of its original removal capacity as shown in Fig. 7. This suggests that the composite material can be used repeatedly for the effective removal of Cr^{6+} ions from effluents.

4 Conclusion

In conclusion, this study investigated the potential of utilizing both AC raw material and polyol in developing a PUAC composite made from coconut industry waste and by-products. This composite proved to be a highly effective adsorbent for removing Cr^{6+} ions from aqueous solutions, as demonstrated in fixed-bed column studies. The results showed that the adsorption capacity in a fixed-bed column set-up was dependent on flow rate and bed height, with higher flow rates resulting in decreased removal capacity and higher bed heights leading to improved removal capacity. Among the models applied to fit the experimental data, the Thomas and Yoon-Nelson models demonstrated a more suitable fitting to describe the breakthrough curves of adsorption processes under different fixed-bed conditions. Additionally, the study revealed that the PUAC can be reused even after four cycles without significantly affecting its adsorption capacity. Further, the successful synthesis of the adsorbent demonstrated the potential of PUAC for the removal of heavy metals in wastewater particularly Cr^{6+} ions in a larger scale.

Conflicts of interest

The authors declare no conflicts of interest.

Acknowledgements

The first author wishes to acknowledge the financial support received from the Philippine government's Department of Science and Technology (DOST), the NICER – Center for Sustainable Polymers of the Mindanao State University – Iligan Institute of Technology for providing the lab facility in the conduct of the study, Jaime Guihawan and Roger Jr Dingcong for their insights and invaluable feedback in writing the manuscript, the Philippine Japan Active Carbon for the provision of coco-shell-based activated carbon, and FABLAB Mindanao for making the fixed-bed column concept possible.

References

1 L. J. Martis, N. Parushuram and Y. Sangappa, *Environ. Sci.: Adv.*, 2022, **1**, 285–296.
2 S. Dutta and R. K. Sharma, *Sep. Sci. Technol.*, 2019, **11**, 371–416.
3 S. Chen, Q. Yue, B. Gao, Q. Li, X. Xu and K. Fu, *Bioresour. Technol.*, 2012, **113**, 114–120.
4 I. Musbah, D. Cicéron, A. Saboni and S. Alexandrova, 2018.
5 F. Parvin, S. Y. Rikta and S. M. Tareq, in *Nanotechnology in Water and Wastewater Treatment*, Elsevier, 2019, pp. 137–157.
6 R. Lakshmipathy and N. C. Sarada, *Environ. Sci.: Water Res. Technol.*, 2015, **1**, 244–250.
7 M. Bhaumik, K. Setshedi, A. Maity and M. S. Onyango, *Sep. Purif. Technol.*, 2013, **110**, 11–19.
8 S. Srivastava, S. B. Agrawal and M. K. Mondal, *Environ. Prog. Sustainable Energy*, 2019, **38**, S68–S76.
9 J. Kotaś and Z. Stasicka, *Environ. Pollut.*, 2000, **107**, 263–283.
10 L. Mukosha, O. S. Maurice and A. Ochieng, *Chem. Eng. Commun.*, 2020, **207**, 1415–1425.
11 M. Sulyman, J. Namiesnik and A. Gierak, *Pol. J. Environ. Stud.*, 2017, **26**, 479–510.
12 S. S. Banerjee, M. V. Joshi and R. V. Jayaram, *Sep. Sci. Technol.*, 2005, **39**, 1611–1629.
13 A. Bakshi and A. K. Panigrahi, *Toxicol. Rep.*, 2018, **5**, 440–447.
14 J. P. Beukes, S. P. du Preez, P. G. van Zyl, D. Paktunc, T. Fabritius, M. Päätalo and M. Cramer, *J. Cleaner Prod.*, 2017, **165**, 874–889.
15 V. Velma, S. S. Vutukuru and P. B. Tchounwou, *Rev. Environ. Health*, 2009, **24**(2), 129–145.
16 S. P. Tembhare, D. P. Barai, B. A. Bhanvase and M. Y. Salunkhe, in *Handbook of Nanomaterials for Wastewater Treatment*, Elsevier, 2021, pp. 575–603.
17 K. Salnikow and A. Zhitkovich, *Chem. Res. Toxicol.*, 2008, **21**, 28–44.
18 S. N. A. Abas, M. H. S. Ismail, L. Kamal and S. Izhar, 2013, 13.
19 Y. Zhang and C. Banks, *Environ. Technol.*, 2005, **26**, 733–744.
20 Z. A. ALOthman, A. Y. Badjah and I. Ali, *J. Mol. Liq.*, 2019, **275**, 41–48.
21 S. Mandal, J. Calderon, S. B. Marpu, M. A. Omary and S. Q. Shi, *J. Contam. Hydrol.*, 2021, **243**, 103869.
22 E. E. Baldez, N. F. Robaina and R. J. Cassella, *J. Hazard. Mater.*, 2008, **159**, 580–586.

23 Y. Lu and R. C. Larock, *Biomacromolecules*, 2008, **9**, 3332–3340.
24 W. He, P. Kang, Z. Fang, J. Hao, H. Wu, Y. Zhu and K. Guo, *Ind. Eng. Chem. Res.*, 2020, **59**, 17513–17519.
25 X. Leng, C. Li, X. Cai, Z. Yang, F. Zhang, Y. Liu, G. Yang, Q. Wang, G. Fang and X. Zhang, *RSC Adv.*, 2022, **12**, 13548–13556.
26 A. Lubguban, R. Malaluan, A. Alguno, A. Tilendo and A. Maputi, Process for the Production of Polyester Polyols and Flexible Polyurethane Foam Derived from Coconut Oil, *Philippine Pat.*, 12021050200, Intellectual Property of the Philippines, 2022.
27 Y.-C. Tu, P. Kiatsimkul, G. Suppes and F.-H. Hsieh, *J. Appl. Polym. Sci.*, 2007, **105**, 453–459.
28 A. Keshavarz, H. Zilouei, A. Abdolmaleki, A. Asadinezhad and A. A. Nikkhah, *Int. J. Environ. Sci. Technol.*, 2016, **13**, 699–710.
29 R. de A. Delucis, W. L. E. Magalhães, C. L. Petzhold and S. C. Amico, *Polym. Compos.*, 2018, **39**, E1770–E1777.
30 D.-M. Guo, Q.-D. An, Z.-Y. Xiao, S.-R. Zhai and Z. Shi, *RSC Adv.*, 2017, **7**, 54039–54052.
31 G. S. Bohart and E. Q. Adams, *J. Am. Chem. Soc.*, 1920, **42**, 523–544.
32 H. C. Thomas, *J. Am. Chem. Soc.*, 1944, **66**, 1664–1666.
33 D. T. Mekonnen, E. Alemayehu and B. Lennartz, *Materials*, 2021, **14**, 5466.
34 Y. H. Yoon and J. H. Nelson, *Am. Ind. Hyg. Assoc. J.*, 1984, **45**, 509–516.
35 A. B. Albadarin, C. Mangwandi, A. H. Al-Muhtaseb, G. M. Walker, S. J. Allen and M. N. M. Ahmad, *Chin. J. Chem. Eng.*, 2012, **20**, 469–477.
36 M. Shoaib Suleman, S. Khan, T. Jamil, W. Aleem, M. Shafiq and N. Gull, *Asian J. Appl. Sci.*, 2014, **2**(5).
37 D. Wu, L. Fang, Y. Qin, W. Wu, C. Mao and H. Zhu, *Mar. Pollut. Bull.*, 2014, **84**, 263–267.
38 A. G. Shirke, P. Desai, M. Vashisht, B. Z. Dholakiya and K. Kuperkar, *J. Surf. Sci. Technol.*, 2020, 125–135.
39 H. Li, L. Liu and F. Yang, *Mar. Pollut. Bull.*, 2012, **64**, 1648–1653.
40 M. Iqhrammullah, Marlina, R. Hedwig, I. Karnadi, K. H. Kurniawan, N. G. Olaiya, M. K. Mohamad Haafiz, H. P. S. Abdul Khalil and S. N. Abdulmadjid, *Polymers*, 2020, **12**, 903.
41 S. J. Eichhorn and W. W. Sampson, *J. R. Soc., Interface*, 2010, **7**, 641–649.
42 G. Nam, S. Choi, H. Byun, Y.-M. Rhym and S. E. Shim, *Macromol. Res.*, 2013, **21**, 958–964.
43 M. Udayakumar, B. El Mrabate, T. Koós, K. Szemmelveisz, F. Kristály, M. Leskó, Á. Filep, R. Géber, M. Schabikowski, P. Baumli, J. Lakatos, P. Tóth and Z. Németh, *Arab. J. Chem.*, 2021, **14**, 103214.
44 W. El Malti, M. Hamieh, A. Noaman, R. Nasser El-Dine, A. Hijazi and W. Al-Khatib, *J. Ecol. Eng.*, 2021, **22**, 99–110.
45 R. G. Dingcong, R. M. Malaluan, A. C. Alguno, D. J. E. Estrada, A. A. Lubguban, E. P. Resurreccion, G. G. Dumancas, H. H. Al-Moameri and A. A. Lubguban, *RSC Adv.*, 2023, **13**, 1985–1994.
46 S. H. Hasan, D. Ranjan and M. Talat, *J. Hazard. Mater.*, 2010, **181**, 1134–1142.
47 P. Kumar and M. S. Chauhan, *J. Environ. Chem. Eng.*, 2019, **7**, 103218.
48 N. Tandon, E. Cimetta, S. Bhumiratana, A. Godier-Furnemont, R. Maidhof and G. Vunjak-Novakovic, *Biomater. Sci.*, 2013, 1178–1194.
49 S. Babel and T. A. Kurniawan, *Chemosphere*, 2004, **54**, 951–967.
50 V. Vinodhini and N. Das, *Am.–Eurasian J. Sci. Res.*, 2009, **4**, 324.
51 T. E. Abilio, B. C. Soares, J. C. José, P. A. Milani, G. Labuto and E. N. V. M. Carrilho, *Environ. Sci. Pollut. Res.*, 2021, **28**(19), 24816–24829.